Analysis and Experimental Demonstration of Possible Architectures for Future Coherent Metro+PON Converged Networks (Post-OFC2024 INVITED)

GIUSEPPE RIZZELLI[1,*], MARIACRISTINA CASASCO[2], VALTER FERRERO[2], ANNACHIARA PAGANO[3], AND ROBERTO GAUDINO[2]

[1] *Photonext Center, Politecnico di Torino, Torino, Italy.*
[2] *Dipartimento di Elettronica e Telecomunicazioni, Politecnico di Torino, Torino, Italy.*
[3] *Telecom Italia, TIM, Italy.*
[*] *giuseppe.rizzelli@polito.it*

Compiled October 4, 2024

We present in this paper a detailed brainstorming on the future option of merging the metro and the passive optical network (PON) access network segments, enabled by the introduction of end-to-end coherent transmission. We begin by reporting the experimental results presented by our group at OFC2024 (for which this paper is an Invited extension). Starting from these preliminary but very promising results, we elaborate on two different possible schematics for metro+PON convergence using edge reconfigurable optical add-drop multiplexers (ROADMs) at the boundary of the two segments, and then we study their physical layer scalability by a mix of experimental characterization and numerical modeling. We show that coherent transceivers enable excellent performance in this scenario, allowing at least 200G per wavelength and even 400G in most cases when traversing all-optically two ROADMs before being routed towards a high splitting ratio PON in the access part of the network. We study several realistic conditions analyzing different bit rates, modulation formats and network architectures, showing the physical layer conditions that would enable PON Optical Distribution Network loss to be in the range from 29 to 35 dB, as required by current international standards. The scalability analysis is first based on link budget and optical signal-to-noise ratio (OSNR) fundamental limitations, and it is then extended considering other physical layer issues, such as tight optical filtering in the ROADMs.

http://dx.doi.org/10.1364/ao.XX.XXXXXX

1. INTRODUCTION

Passive Optical Network (PON) is today the ubiquitously used solution for fixed optical access, in particular for Fiber-to-the-Home (FTTH), with an installed base worldwide that was recently estimated to have surpassed one billion terminations. Consequently, ITU-T and IEEE are continuously working to ratify new standards for increasing bit rates. In 2021, ITU-T released 50G-PON (G.9804.1, [1]) for 50 Gbps downstream (DS) and 12.5/25 Gbps upstream (US, with a provision for upgrade to 50 Gbps US). The involved ITU-T Study Group 15 (G.Sup.VHSP) is currently brainstorming for the next steps towards higher bit rates. Among the different discussed options on the bit rate per wavelength [2, 3], one is 100 Gbps intensity-modulation and direct-detection (IM-DD) where IM-DD would need to be stretched to its ultimate physical layer limits in terms of link budget and chromatic dispersion, so that strong digital signal processing (DSP) would be needed for FEC and pre and/or post equalization. Another option under discussion in G.Sup.VHSP is 200 Gbps using advanced modulation formats (PM-QAM family) and coherent detection. This second option, today widely popular for long reach transport networks and for significantly higher bit rates, would require a strong technological revolution, since coherent transceivers seems today too expensive for the access ecosystems. It is expected anyway that coherent transceivers cost may significantly decrease, a trend that can strongly depend on what will happen in the data center interconnect (DCI) segment. Overall, considering that next generation PON schemes may enter the PON market in 7-8 years from now, the research in coherent PON is today very timely and, thus, very active.

In our opinion, the introduction of coherent transceivers in the PON ecosystem will be justified if it will enable not only a mere increase in bit rate but also other "added values", such as longer reach, higher splitting ratio i.e a higher number of Optical Network Units (ONUs) per PON tree, and higher network-layer flexibility. In this paper, we elaborate on all these options,

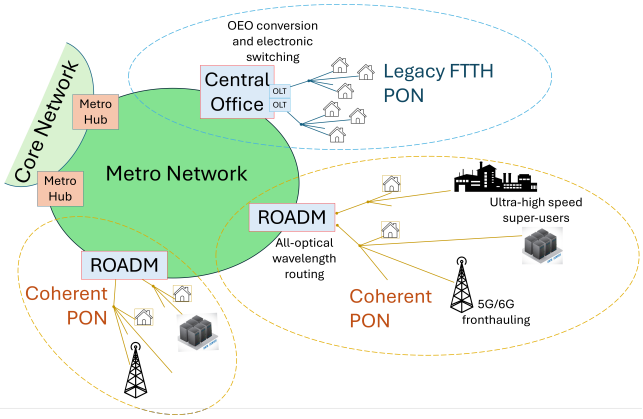

Fig. 1. General schematic of converged metro+PON networks.

proposing and discussing in detail, both experimentally and by theoretical scalability analysis, an all-optical convergence between the metro and the PON segments, enabled by coherent transmission and the use of Reconfigurable Optical Add-Drop Multiplexers (ROADM) at the boundary of the two segments, as schematically depicted in Fig.1. This manuscript is a post-OFC2024 invited paper that largely extend our preliminary work presented at the conference in [4]. We believe that coherent PON is just at the beginning of a large research effort, as can be seen from the very large number of papers on the topic accepted in recent Conferences, so that it is a very good moment to propose new advanced and somehow "far fetched" studies, such as the one that we will discuss in this paper. The potential applications of these super-high capacity ligthpaths over PON will likely not be required for FTTH (for which it is very difficult to envision any request above about 1 Gbps per household), but for future PON "super-user" terminals such as:

- fronthauling (or in general X-hauling) for 5.5G and future 6G mobile, in particular if and when massive MIMO and very large RF bandwidths are introduced in the wireless segment
- new applications requiring super-high speed connection in a single location, such as medium size data centers inside urban areas or new industrial applications.

The paper is organized as follows. In Sect. 2, we shortly summarize our work presented in [4] to introduce a preliminary experimental demonstration of metro+PON convergence. In Sect. 3, we propose two different solutions for metro+PON convergence using edge-ROADMs: a "disruptive architecture" where all PON ONUs use only coherent transmission, and an "evolutionary architecture" based on a mix of legacy ONUs and coherent ONUs. In the following Sect. 4, we present an extensive scalability study, which we believe it is the main new contribution of this paper as an extension of our work in [4]. In particular, in Subsection A we characterize experimentally several commercial coherent transceiver and then we use these measurements to validate the analytical model presented in [5], that allows to predict coherent transmission performance vs. received optical power (ROP), optical signal to noise ratio (OSNR) and filtering impairments. This analytical approach is then extensively used for a scalability analysis of the disruptive architecture (in Subsection B) and of the evolutionary architecture (in Subsection C). While this scalability analysis will consider only power budget

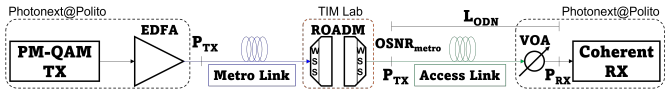

Fig. 2. Experimental setup of the coherent metro-access network based on laboratory equipment with lumped components (see [4] for more details).

and OSNR limitations, the following Sect. 5 will consider the impact of some additional impairments, such as tight optical filters in ROADMs or limited optoelectronic bandwidth in the transceivers. Finally, we will draw some conclusion in Sect. 6.

Here, we point out the main assumptions that we will make in the rest of the paper. We will present mostly physical layer considerations based on the current performance of commercial single-carrier coherent transceivers using PM-QAM modulation (we will then mostly focus on solutions enabling 200G per wavelength using PM-QPSK, and 400G using PM-16QAM). The experiments and the following scalability analysis will be focused on the fundamental limitations given by the coherent transceivers in terms of BER vs. OSNR and ROP. In fact, as we will discuss in detail, the usual characterization in terms of BER vs. OSNR only is not sufficient for the architectures under discussion here, since in the DS direction the coherent receivers may operate at very low ROP, so that BER will be limited by a mix of ASE noise (introduced by the EDFAs in the edge ROADMs for the metro part) and the internal transceiver noise (see [5] for a detailed discussion on this).

We assume two different transparent wavelengths for each PON and for each of the two directions (λ_i^{DS} and λ_i^{US}) and TDM/TDMA multiplexing: this is clearly not yet a commercially available solution for coherent transceivers, but many recent papers are reporting experimental demonstration of the required burst mode coherent hardware and DSP [6], showing very promising results. As usual in this respect, downstream is not critical, since transmission and detection, even when using TDM, is time-continuous, while the challenge is the upstream direction, which should be based on TDMA in burst-mode for both transmission and detection, unless specific architectures are considered where the ultra high speed coherent lambda pair has to reach a single PON destination (i.e. point-to-point over PON). An alternative to TDM/TDMA would be based on the use of a Digital Subcarrier Multiplexed (DSCM) transceiver, which has been recently proven [7] to allow transmission on the same wavelength simultaneously for both US and DS and to be compliant with PON high optical distribution network (ODN) loss, as we will mention in the final discussion in Sect. 6,

2. PRELIMINARY EXPERIMENTAL RESULTS ON METRO+PON DOWNSTREAM (FROM OFC2024)

We report here a summary of the the main results we presented in our OFC2024 paper [4], of which this JOCN paper is an invited extension. Fig. 2 shows the block diagram of the experiment we used to demonstrate downstream coherent metro-access transmission. The transmitter, located in our PhotoNext lab, is composed of a 92 GS/s arbitrary waveform generator feeding electrical data signals amplified through electrical driver amplifiers to a 35 GHz bandwidth Dual-polarization In-phase/Quadrature Mach-Zehnder modulator, followed by an erbium doped fiber amplifier (EDFA) with 5 dB noise figure to amplify the transmitted PM-16QAM signal up to $P_{TX} = 11$ dBm at the input

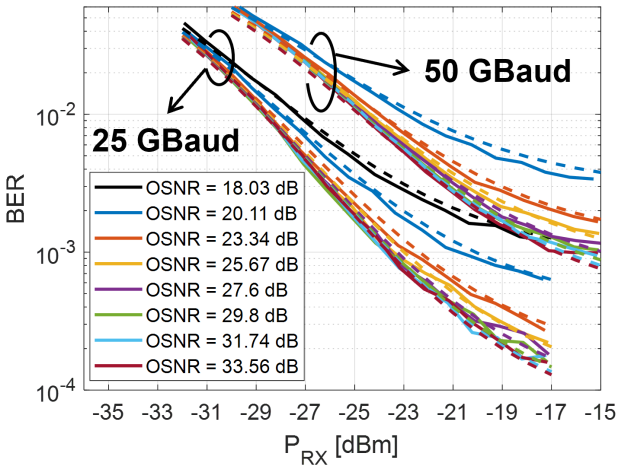

Fig. 3. a) Experimental (solid) and analytical (dashed) BER vs P_{RX} at different $OSNR_{metro}$ for 25 and 50 GBaud PM-16QAM for the setup shown in Fig. 2 [4].

of the metro section, made of a 16.5 km metropolitan G.652 fibers deployed in the city of Turin, Italy. Although the propagation distance is not comparable to realistic metro configurations, the total 15 dB attenuation introduced on the optical path by patch panels and inter-connection points, make the overall power budget similar to what could be expected in a metro link. On the other end of the link, in the TIM lab, we used a commercial ROADM node to all-optically merge the metro and the the access section of the network. The ROADM routes and filters the downstream signal through two wavelength selective switches (WSS) and EDFAs. Each WSS introduces a 5 dB attenuation for about 10 dB overall insertion loss of the ROADM. We programmed the ROADM internal variable optical attenuators (VOA) to obtain $P_{TX} = 11$ dBm (the highest launched power values in current PON standards, such as XG-PON) and to set a variable $OSNR_{metro}$ at the input of the PON access segment, which is made again of 16.5 km of deployed fiber and a VOA to emulate a PON. At the end of this link, the received optical signal is coherently detected through a 40 GHz bandwidth commercial coherent receiver (Neophotonics), digitized through a 200 GS/s Tektronix real-time oscilloscope and off-line processed through a standard DSP chain. A variable optical attenuator (VOA) at the receiver input is used to vary the received optical power P_{RX} and measure the BER vs P_{RX} curves for different $OSNR_{metro}$ values (defined on a bandwidth equal to the symbol rate). The total ODN loss L_{ODN} is computed as the difference between the transmitted power P_{TX} =11 dBm and P_{RX}. The sensitivity curves for a gross 400G transmission based on 50 GBaud PM-16QAM modulation and a gross 200G solution based on 25 GBaud PM-16QAM are depicted in Fig. 3 for different $OSNR_{metro}$ values. The figure shows a comparison between the experimental (solid) curves and an analytical (dashed lines) fitting, obtained using a previously developed analytical model [8] based on parameter extraction (further details about the model can be found in [8–10]). Here we just mention that the analytical approach is based on the computation of the equivalent signal-to-noise ratio (SNR) on each of the coherent receiver four quadrature outputs as:

$$SNR_{RX} = \frac{P_{RX}}{\frac{\sigma^2_{th}}{P_{LO}} + P_{LO}\cdot\sigma^2_{n_{LO}}\cdot CMRR + \sigma^2_{shot} + \frac{P_{RX}}{SNR_Q} + \frac{P_{RX}}{OSNR_{metro}}} \quad (1)$$

where P_{RX} is the received average signal optical power, P_{LO} is the continuous wave (CW) optical power of the local oscillator (LO), $OSNR_{metro}$ is the OSNR defined on a bandwidth equal to the symbol rate at the edge between the metro and the PON segment, $CMRR$ is the Common Mode Rejection Ratio of the balanced photodetector, $\sigma^2_{n_{LO}}$ is the variance of the LO relative intensity noise (RIN) contribution, σ^2_{th} is the variance of the transimpedence amplifier (TIA) thermal noise, σ^2_{shot} is the variance of the shot noise generated in the photodetection process and the SNR_Q parameter accounts for other signal power-independent implementation penalties such as quantization noise, phase noise and imperfect constellation generation. The main noise contribution terms can be computed as

$$\sigma^2_{th} = \frac{i^2_{TIA}\cdot B^{RX}_{eq}}{8\cdot R^2};\quad \sigma^2_{shot} = \frac{q\cdot B^{RX}_{eq}}{2\cdot R};\quad \sigma^2_{n_{LO}} = RIN\cdot\frac{B^{RX}_{eq}}{2} \quad \textbf{(2)}$$

where R is the coherent receiver responsivity (in A/W) including the passive losses before the photodiodes, i_{TIA} is the input-referred noise current density (IRND in $pA/\sqrt{Hz}$) of a single transimpedance amplifier, B^{RX}_{eq} is the effective noise bandwidth of the receiver, q is the electron charge and RIN is the LO RIN parameter.

To refine the analytical tool used in Fig. 3, we numerically extracted the four parameters i_{TIA}, $CMRR$, R and SNR_Q through fitting between the analytical BER values obtained converting SNR_{RX} through the theoretical formula, and the experimental BER measured at the highest OSNR for the lowest 25 GBaud symbol rate. The fitting procedure is based on the minimization of the mean squared error between the experimental and analytical BER values. We then used the same obtained values ($i_{TIA} = 20.73\cdot 10^{-12}[A/\sqrt{Hz}]$, $CMRR = -18.35$ dB, $R = 0.067$ A/W and $SNR_Q = 17.7$ dB) to compute the analytical sensitivity curves for the other OSNR and symbol rate values. Fig. 3 shows a remarkable agreement of the model with the experiment in all the considered cases. We observe that, especially for the 400G transmission, the sensitivity can hardly reach $BER = 10^{-3}$, highlighting that an advanced forward error correction (FEC) algorithm is needed in this kind of metro+PON solution. Thus, hereafter we will focus mainly on the two BER thresholds $BER_T = 10^{-2}$ and $BER_T = 2\cdot 10^{-2}$ ssuming the use of a generic hard decision FEC (HD-FEC) with 14.5% overhead and a generic soft decision FEC (SD-FEC) with 15.3% overhead, respectively. Using our analytical model, we show in Fig. 4 the scalability analysis for the achievable ODN loss at the two BER thresholds for three different modulation formats providing 200G through 50 GBaud PM-QPSK modulation, 400G with 50 GBaud PM-16QAM modulation and 300G with 25 GBaud PM-64QAM modulation (which we selected to analyze also an option at low baud rate, but at high QAM cardinality). Although other, more advanced, modulation options such as probabilistic shaping might be available, we have focused on the "classical" approach to obtain a benchmark of the coherent technology performance without adding extra complexity and, as a consequence, extra cost to the metro-access solution. In this analysis all the considered bit rates are gross bit rates. The 400G curves show a very good match of the model with the experiment and demostrate that a very high L_{ODN} above 30 dB can be expected even when we scale the OSNR down to 15 dB and 18 dB, respectively for HD-FEC and SD-FEC. Moreover, analytical extrapolation shows extremely high performance at any considered OSNR levels with L_{ODN} in excess of 40 dB for 200G PM-QPSK, whereas significantly lower L_{ODN} is achievable for

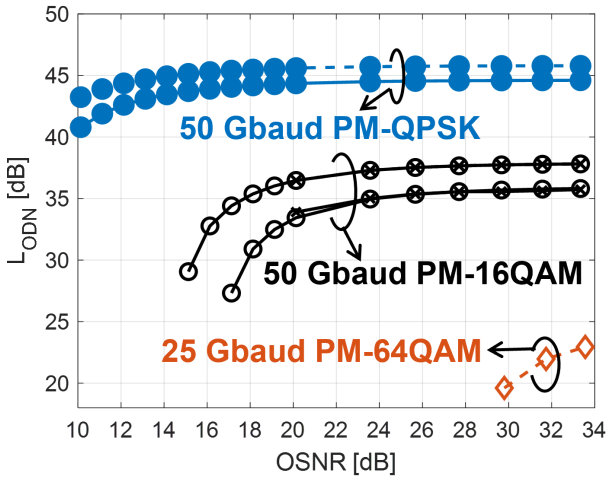

Fig. 4. ODN loss vs. $OSNR_{metro}$ at $BER = 10^{-2}$ (solid) and $BER = 2 \cdot 10^{-2}$ (dashed) for analytical 50 GBaud PM-QPSK (blue, dots), analytical (circles) and experimental (crosses) 50 GBaud PM-16QAM (black) and analytical 25 GBaud PM-64QAM (orange, diamonds).

the 300G PM-64QAM case.

The experimental and scalability results shown in this Section and taken from our OFC2024 paper [4] were reported here to preliminary introduce the topic of metro+PON convergence. In the following Sections, we largely extend the scope of our research and the novelty of this paper compared to [4] along the following directions:

- examining the performance of three different commercial coherent transceivers;
- considering more realistic ROADM architectures, proposing two different configurations (each with two variants);
- obtaining a comprehensive set of scalability curves.

3. THE PROPOSED ARCHITECTURES FOR METRO+PON CONVERGED NETWORKS

In this Section, we propose two different architectures for metro+PON convergence, both based on edge ROADMs at the boundary of the two segments. We believe that these two architectures are reasonable examples of how a metro+PON network can be organized, but obviously many other variants are possible and, we are sure, will be proposed in the near future. In fact, metro+PON convergence is a quite new field, and our goal in this paper is to start analyzing the "tip of the iceberg" with a first set of examples and scalability analyses. In particular, we propose and analyze the following two architectures:

1. one where PON US and DS transmission is exclusively based on coherent technologies, without any legacy IM-DD standards. We will indicate this option as the "Disruptive Architecture" (D-ARCH) in the rest of the paper
2. another where PON uses a mix of legacy IM-DD and coherent transmission, indicating it as the "Evolutionary Architecture" (E-ARCH)

In both cases, we assume (see Fig. 5) that the key building block of each metro node based on ROADMs is the concatenation (for each degree, i.e. for each "direction") of an EDFA and a completely programmable WSS. Moreover, we assume that all WSS inputs and outputs are connected by an optical matrix. We anticipate that in our physical layer scalability analysis, the optical attenuation introduced by the WSS and connection matrix will be of paramount importance. Fig. 5 shows the detailed block diagram of the D-ARCH system, which is based on edge ROADMS of degree 3 (hereafter indicted as 3D ROADM): two degrees (D1 and D2 green labels in the schematics) are, as it is today very common, used in a ring-like metro network for routing the lightpaths on the set of wavelengths $\overrightarrow{\lambda}_j^{metro}$ and $\overleftarrow{\lambda}_j^{metro}$ dedicated to metro traffic flowing in the two directions, while the third degree (D3) is used to route wavelengths toward the access PONs on wavelengths λ_i^{DS} and λ_i^{US} for the access US and DS traffic, one wavelength pair per PON tree. We further assume that the wavelengths that are to be routed to the access part are generated in the DS (on the set of wavelengths λ_i^{DS}) and received in the US (on the set of wavelengths λ_i^{US}) in the first node labelled ROADM1, then they travel together with other wavelengths used for metro traffic though ROADM2 and finally, in ROADM3, they are all-optically routed towards n PON trees, using one wavelength per direction per PON. In Fig. 5, the blocks involved in DS transmission are in solid black, those for US are in dashed red while the wavelength dedicated to metro traffic are in magenta.

The architecture shown is Fig. 5 and the following scalability study assume propagation over three metropolitan ROADM nodes: this is meant to be a reasonable example, also considering that, for instance for fronthauling applications, especially in urban and dense urban areas, the end-to-end transmission distance cannot be too long, due to latency constraints. Clearly, different metro configurations can be conceived, but obviously it is not possible to analyze all of them in a single paper. However, we will show that the ultimate physical layer limitations is a combination of OSNR available in the metro segment, and ROP in the access segments: this key result could be applied in future analysis to much more general metro architectures, and in particular to much longer metro networks comprising several nodes (and also longer fibers, if latency is not an issue). In fact, it is today widely accepted that the generalized OSNR (G-OSNR) is a very good general metric to analyze, in longer distance networks, not only ASE noise impact, but also fiber Kerr and Raman nonlinearities. Thus, results presented in the following sections such as those in Fig. 9 (BER countour plots vs. ROP and OSNR) can easily be used in terms of the generalized OSNR available in the metro segment, allowing our result to be applicable to a much broader range of situations compared to the one we considered as an example in Fig. 5.

As a variant of the D-ARCH, Fig. 6 shows an alternative solution based on 2D ROADMs (for the two metro directions), where the third degree D3 is replaced by a single WSS and a bank of Semiconductor Optical Amplifiers (SOAs) for each output line. We decided to study this alternative scheme since, as we will show in the next Section, it has potentially better scalability performance.

The other proposed evolutionary E-ARCH system is shown in Fig. 7, where we assume a co-existence of legacy PON (such as GPON, XG-PON and/or 50G-PON) wavelengths and terminals with the wavelengths for super-high speed coherent transmission, enabled by a suitable wavelength allocation plan.

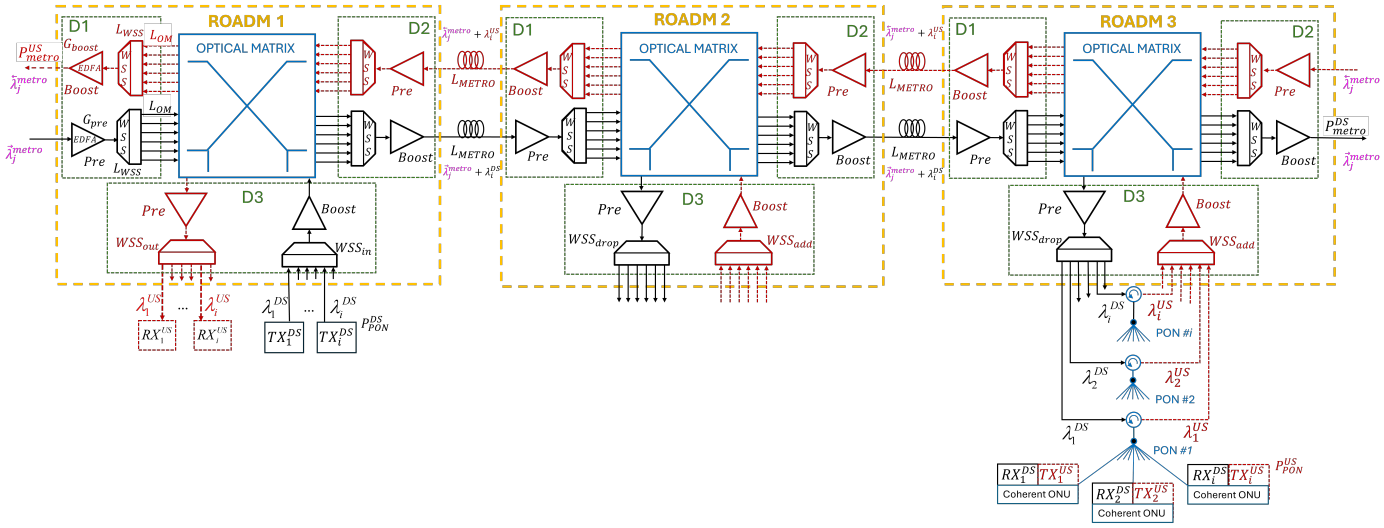

Fig. 5. Schematic for the disruptive architecture (D-ARCH) based on 3D ROADMs.

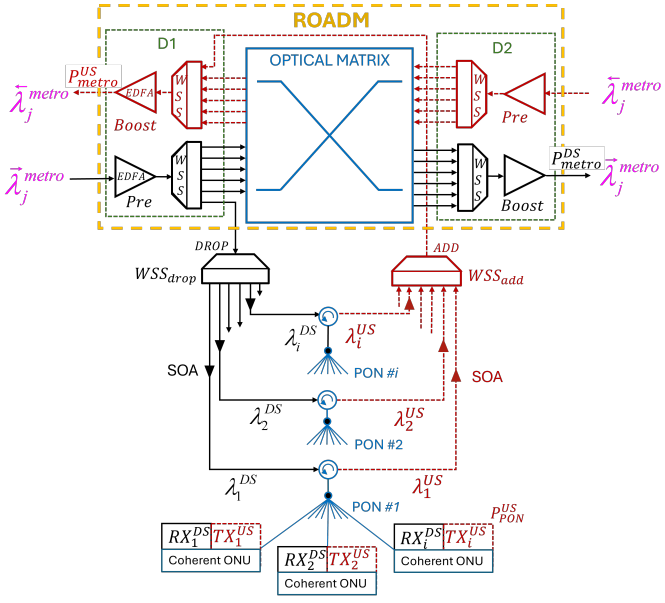

Fig. 6. 2D ROADM solution for the disruptive architecture where the WSS+SOAs replace the third degree of the 3D ROADM D-ARCH solution.

In particular, starting with the DS direction, we assume that a wavelength λ_{coh}^{DS} is generated in the metro in a previous "source" node and is then used (in TDM) both for an electronic switch feeding an array of legacy optical line terminals (OLTs) TX and also for a PON requiring a super-high speed connection to some of its super-user ONUs. Similarly, in upstream a wavelength λ_{coh}^{US} is used for both the traffic generated by the electronic switch and directed to the metro network, and for the one coming for the US of some super-user ONUs. As in the previous schematics, the solid black line represents the DS direction while the dashed red is the US direction. Also for E-ARCH, we will analyze the two variants shown in Fig. 7 for 2D and 3D ROADMs.

4. SCALABILITY ANALYSIS OF THE PROPOSED METRO+PON ARCHITECTURES

This is the central Section of this paper, and it is focused on presenting the scalability of the D-ARCH and E-ARCH solutions focusing on the fundamental physical layer limitations induced on coherent transmission by optical amplifiers ASE noise, coherent transceiver internal noise and several lossy optical components that are present in both the metro and PON segments and inside the ROADM. Other possible impairments will be discussed in the following Sect. 5. We strive to introduce in our models practical and realistic physical layer parameters for the ROADMs (using data taken from commercial ROADMs datasheets), splitters and fiber losses and for the coherent transceivers characteristics in terms of BER vs. ROP and OSNR. Since this last point is absolutely fundamental in our analysis, we start with a dedicated set of experiments on transceiver characterization in the following Subsection A.

A. Experimental characterization of coherent transceivers vs. OSNR and ROP

In this Subsection, we present the experimental characterization of the performance of several commercial coherent transceivers as a function of both OSNR and ROP at its receiver input and then we match the experimental results with an analytical model that is key for the scalability analysis in the remainder of the paper. We experimentally measured three different commercial transceivers produced by three different manufacturers (that we

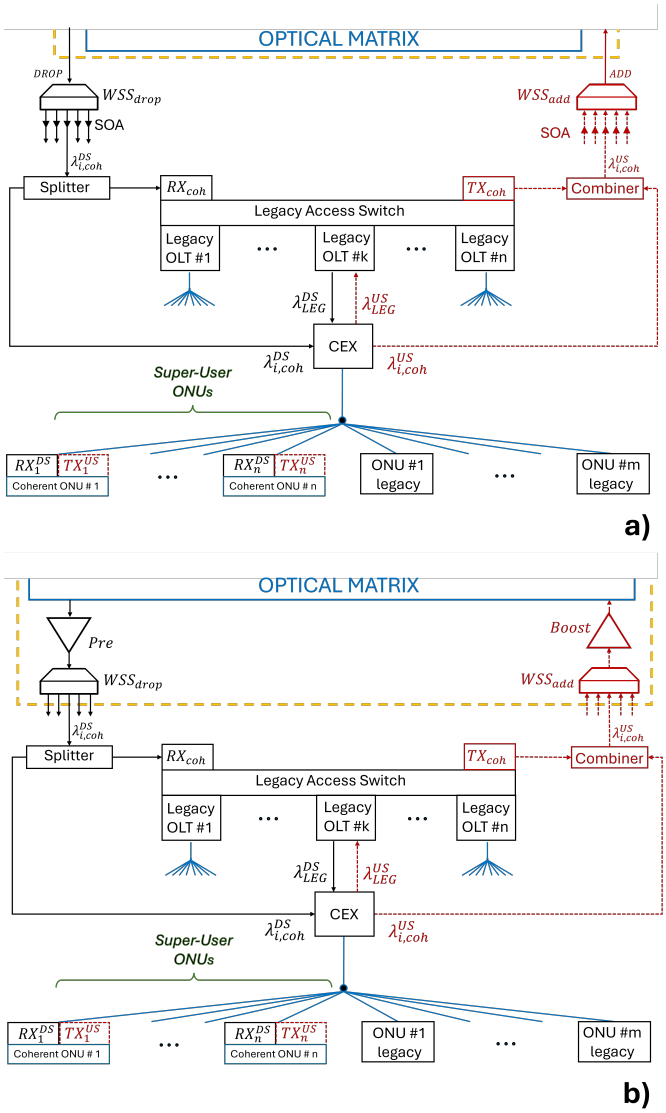

Fig. 7. Evolutionary architecture (E-ARCH) based on a) 2D ROADM and b) 3D ROADM.

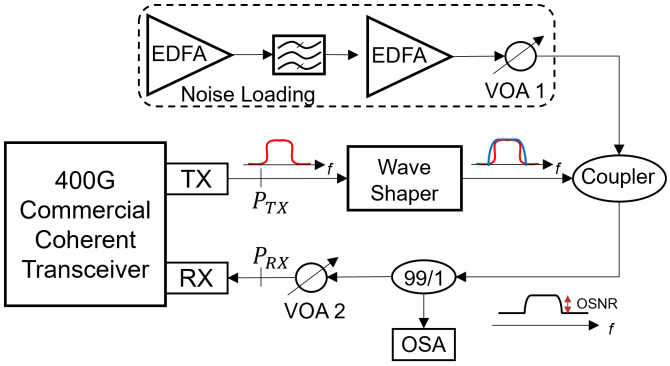

Fig. 8. Experimental setup for the TRX characterization with noise loading.

will cindicate as "Vendor 1", "Vendor 2" and "Vendor 3") and then we show in Fig. 9 the resulting sensitivity as a function of the received optical power for different OSNR levels for 400 Gbps net bit rate corresponding to 63 Gbaud symbol rate transmission with PM-16QAM modulation, a higher overall baud rate than what we used in Section 2 and [4]. This characterization was performed on the setup shown in Fig. 8, where the TRX output is filtered through a Finisar 1000S programmable waveshaper to emulate the ROADM WSS in Fig. 2 (the filtering penalties will actually be mostly studied in the following Sect. 5). Then a standard noise loading technique is used to generate amplified spontaneous emission (ASE) noise, whose level can be adjusted acting on VOA1 to set a desired OSNR level. Before the receiver, VOA2 is used to vary again the received optical power P_{RX}. The OSNR (defined on a bandwidth equal to the baud rate) is measured through an optical spectrum analyzer (OSA) at the receiver input. In this experiment, we did not consider fiber propagation operating the system in a back-to-back (BtB) configuration.

Fig. 9 shows, as expected, slightly different performance of the three TRX, particularly in terms of BER vs. ROP. Focusing on the sensitivity at $BER_T = 10^{-2}$ "Vendor 1" TRX in Fig. 9a is the best performing one, with a required minimum P_{RX} around -25 dBm at the highset OSNR, while "Vendor 2" (Fig. 9b) and "Vendor 3" (Fig. 9c) TRX require -22 dBm and -23 dBm, respectively. Moreover, "Vendor 1" TRX also performs better at lower BER levels, being able to provide $BER = 10^{-4}$ whereas the other two TRX display a higher BER floor.

The experimental sensitivity curves were then used to validate an analytical model for performance prediction on an even larger set of optical parameters, and in Fig. 9 we present the resulting analytically obtained sensitivity curves using dashed lines, showing a very good accuracy for the BER of interest, i.e. those above 10^{-3}. As the model used in 2 and [4] requires a complete characterization of an entire sensitivity curve for the extraction of the four main parameters, in this new analysis of different TRX performance we decided to test the applicability of another analytical model that only requires the knowledge of the spectral profile of the signal and of the filtering stages, if any. The model has been presented and validated against simulations and experiments many times for both coherent and direct detection systems and details on its derivation can be found in [5, 11–14]. Here we only mention that this model is based on the computation of a spectrally resolved SNR as:

$$SNR(f) = \frac{PSD_S(f)}{PSD_N(f)} = \frac{\frac{P_{RX}}{R_S} \cdot |H_{Tot}(f)|^2}{N_0 + PSD_{ASE}(f) + \frac{P_{RX}}{R_S \cdot SNR_Q}} \quad (3)$$

where $PSD_S(f)$ is the PSD of the useful signal and $PSD_N(f)$ is the PSD of the noise, $|H_{Tot}(f)|^2 = |H_{TX}(f)|^2 \cdot |H_{CH}(f)|^2 \cdot |H_{RX}(f)|^2$, with $|H_{TX}(f)|^2$ the PSD of the transmitted signal, $H_{CH}(f)$ the transfer function of the channel (e.g. when the channel bandwidth is limited by the ROADM at the edge between the metro and access sections of the network, or by the WaveShaper filter our experiments) and $H_{RX}(f)$ the frequency response of the coherent receiver. R_S is the symbol rate, N_0 is the PSD of the noise generated inside the coherent receiver (typically shot noise and transimpedence amplifier thermal noise), $PSD_{ASE}(f) = \frac{P_{RX}}{OSNR} \cdot |H_{RX}(f)|^2$ is the PSD of the ASE noise induced by the optical amplification and SNR_Q is again the SNR that takes into account the implementation penalties responsible for the BER floor in the BER vs. P_{RX} curves. Then, the SNR at the coherent receiver equalizer output, assuming an (infinitely

long) feedforward equalizer (FFE) [15] is

$$SNR = \left(T \cdot \int_{-\frac{1}{2T}}^{\frac{1}{2T}} \left(1 + \overline{SNR}(f)\right)^{-1} df \right)^{-1} - 1 \quad (4)$$

where $\overline{SNR}(f)$ is the folded version of $SNR(f)$

$$\overline{SNR}(f) = \sum_{\mu} SNR\left(f - \frac{\mu}{T}\right) \quad (5)$$

μ is the integer number of spectral foldings, and T is the symbol period.

Also in this case, the agreement of the analytical model with the experiment is excellent, especially for high BER levels around 10^{-2}. We only observe a slight deviation for low BER values when the model overestimates the performance. We ascribe this effect to a non-perfect optimization of the equalizer parameters inside the TRX DSP. Such a limitation is not taken into account by the model as it is based on a sort of ideal estimator with an infinite number of equalizer taps. Conversely, the DSP implemented on the application-specific integrated circuit of the TRX has a finite number of taps, that is usually set to the lowest possible value to simplify the circuit design and minimize the associated power consumption.

This model is simpler than the one used in 2 and [4] as it does not involve a full characterization of the BERvsP_{RX} curve, but it only requires information about the spectral features of the transceiver and the channel, still providing excellent accuracy. Thus, in the following Sections we assume the metro+PON system is equipped with "Vendor 3" TRX (the TRX for which we obtained the best match between analytical and experimental results), and we use the results shown in Fig. 9c as the starting point for a scalability analysis of the architectures introduced in Sect. 3 that we envision as possible configurations of the metro+PON converged network. Moreover we selected the "Vendor 3" TRX, since it provides intermediate performance with respect to "Vendor 1" and "Vendor 2" TRX. The experimental and analytical performance of "Vendor 3" TRX at the two BER thresholds of interest are depicted in Fig. 10, where estimation errors lower than 0.5 dB can be observed in both cases for OSNR values down to 18 dB. For lower OSNR the estimation error increases to about 1.2 dB due to the limitations in the TRX DSP previously discussed.

B. Scalability Analysis for the Disruptive Architectures

In this Subsection, we study the scalability at the physical layer of the D-ARCH schematics proposed in Subsection B using the experimental measurements for "Vendor 3" TRX and the previously described analytical tool. In particular, we will present a scalability analysis of the DS and US transmission for 63 GBaud PM-QPSK and 63 GBaud PM-16QAM signals for net 200G and 400G all-optical, full-coherent metro+PON solutions and under several realistic assumptions for optical loss and noise.

As described in Section 3, we will focus the study on the two variants (3D and 2D edge-ROADMS) for the D-ARCH architecture. The former ("3D D-ARCH") assumes the use of ROADMs of degree 3 where the add and drop paths for the coherent PON lambdas cross an EDFA and a WSS in the order shown in Fig. 5 for the DS (black path) and US (red path) directions. The latter ("2D D-ARCH"), on the other hand, is a solution that we investigate to determine whether a more cost-effective solution can be put in place employing degree 2 ROADMs and replacing the amplification stage of the whole PON wavelength bundle through EDFAs with one SOA for each individual lambda.

In our analysis, we assume a maximum fiber transmitted power on the metro segment $P^{DS}_{metro} = P^{US}_{metro} = 0$ dBm per wavelength, a maximum transmitted power on the PON section $P^{DS}_{PON} = 11$ dBm in DS direction and $P^{US}_{PON} = 5$ dBm in US at the ONU transmitter output. Each degree of the ROADM consists of a preamp $EDFA_{pre}$ with gain G_{pre} and a WSS in one direction and another WSS and a booster $EDFA_{boost}$ with gain G_{boost} in the other direction; these two gains will be varied inside reasonable ranges in the following analysis. Moreover, we assume that 40 WDM wavelengths travel on the metro network (some of which are then directed by the edge-ROADM towards the access network, while others are assumed to be used for metro traffic), thus the maximum output power of the $EDFA_{pre}$ must be equally split on each λ. As anticipated, our goal is to use realistic parameters as indicated in commercial ROADM datasheets, thus we assume here that the maximum output power for the preamp EDFA is 22 dBm and therefore at the output of $EDFA_{pre}$ the maximum possible average optical power is 6 dBm per each of the 40 channels. A different assumption on the total number of channels would thus affect the per-channel power levels achievable in different points of the analyzed network configuration, whereas it would not impact the wavelength allocation assumed in accordance with the ITU-T 100 GHz grid [16]. However, the wavelength management plan needs to be carefully designed to take into account the number of metro channels, the number of PON trees, the number and location of the coherent super-users and the limitations associated with the power unbalance introduced by uneven amplification and propagation effects across

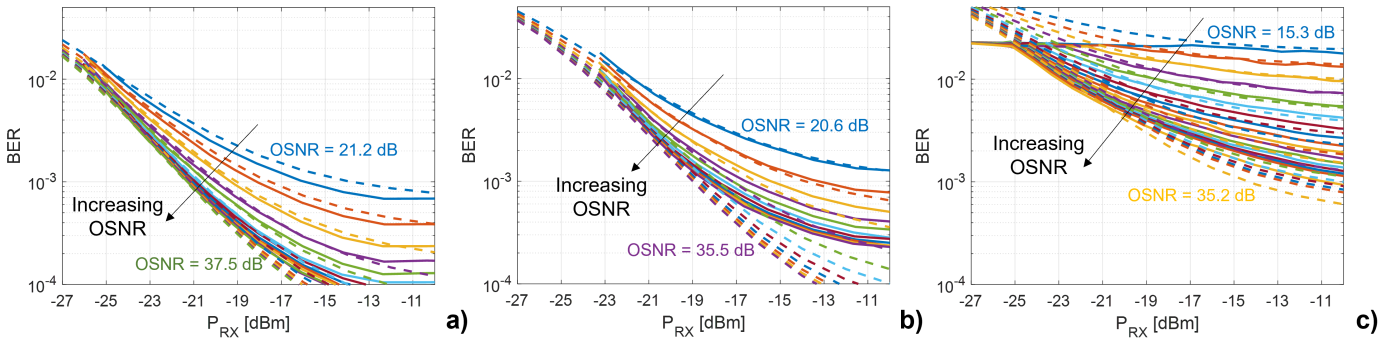

Fig. 9. Experimental (solid) and analytical (dashed) BER vs P_{RX} at different $OSNR$ levels for a) "Vendor 1" TRX, b) "Vendor 2" TRX, c) "Vendor 3" TRX.

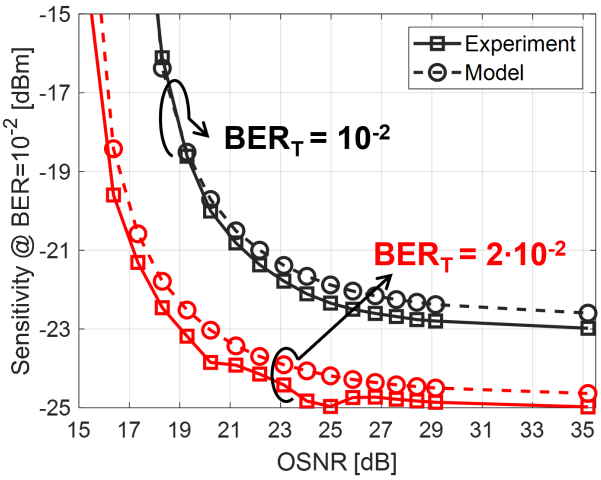

Fig. 10. Experimental (solid, squares) and analytical (dashed, circles) sensitivity vs. $OSNR$ at $BER = 10^{-2}$ (black) and $BER = 2 \cdot 10^{-2}$ (red) for "Vendor 3" TRX at 400G PM-16QAM.

the C-band. For the evolutionary architecture the wavelength plan should also be based on a strict compatibility with the used legacy PON standards.

After the amplification stage at the ROADM input, each λ is attenuated by the chain of a WSS, an optical matrix and another WSS. We assume a 5 dB insertion loss L_{WSS} for each WSS and a variable optical matrix loss L_{OM}, since this parameter strongly depends on the used switching technology and, as we will show, may significantly impact the performance of the analyzed transmission systems. Under some extreme conditions with very high L_{OM} values, the per-channel power at the input of the booster amplifier might be extremely low, requiring high G_{boost} values to have again $P_{metro} = 0$ dBm at the input of the next metro fiber link. The attenuation introduced by the optical matrix is, therefore, a key parameter of the metro+PON system. Thus, we will show the results of our analysis in terms of the achievable L_{ODN} also as a function of the L_{OM} parameter. Throughout the manuscript the loss introduced by the metro link fiber is assumed to be $L_{metro} = 10$ dB (about 40-50 km propagation distance on the metro path) and $G_{pre} = 16$ dB to get 6 dBm per channel at its output. We do not consider fiber transmission impairments (such as Kerr nonlinearity or chromatic dispersion) since the distance to be covered in a metro+PON environment will likely be limited (to avoid excessive latency as required for instance by fronthauling or for several other ultra-low latency applications). We also recognize that we neglect other possible physical layer impairments (such as non flat EDFA gain or noise figure). In fact, we remind, as we discussed in the Introduction, that this paper is a first preliminary study in the emerging area of the architecture and scalability of metro+PON network, so all second-order effects will for sure be worth considering in future works.

In this analysis, we used our analytical model to compute a frequency-resolved $SNR(f)$ as in Eq. 3. In both the "2D" and "3D" disruptive architectures and in both DS and US direction, the signal travels through six WSSs, two for each of the three involved ROADMs. We thus have:

$$|H_{Tot}(f)|^2 = |H_{TX}(f)|^2 \cdot |H^{WSS}(f)|^2 \cdot |H^{WSS}(f)|^2 \cdot |H^{WSS}(f)|^2 \cdot |H^{WSS}(f)|^2 \cdot |H^{WSS}(f)|^2 \cdot |H^{WSS}(f)|^2 \cdot |H_{RX}(f)|^2 \quad (6)$$

where $H^{WSS}(f)$ is the transfer function of each WSS, assumed to have a supergaussian profile of order 3 and bandwidth B equal to 150% of the symbol rate R_S, a value that was selected to have negligible penalty due to optical filtering, since this topic will be addressed in the following Sect. 5. In contrast, the PSD of the ASE noise depends on the type and number of amplifiers crossed by the signal in each network configuration and is thus different in each case. For instance, focusing on the DS direction of the proposed "3D" scheme the contribution of the first three EDFAs is

$$\begin{aligned} PSD_{ASE}(f) = \Bigg[& hf_c(G_{boost} - 1)F \cdot \frac{G_{pre}}{L_1^{ROADM}} \cdot \frac{G_{boost}}{L_{metro}} \\ & \cdot \frac{G_{pre}}{L_2^{ROADM}} \cdot \frac{G_{boost}}{L_{metro}} \cdot \frac{G_{pre}}{L_3^{ROADM}} \cdot \frac{1}{L_{WSS} \cdot L_{Circ} \cdot L_{ODN}} \\ & \cdot |H_{WSS}(f)|^2 \cdot |H_{WSS}(f)|^2 \cdot |H_{WSS}(f)|^2 \cdot |H_{WSS}(f)|^2 \\ & \cdot |H_{WSS}(f)|^2 \Bigg] + \Bigg[hf_c(G_{pre} - 1)F \cdot \frac{G_{boost}}{L_{metro}} \cdot \frac{G_{pre}}{L_2^{ROADM}} \cdot \frac{G_{boost}}{L_{metro}} \\ & \cdot \frac{G_{pre}}{L_3^{ROADM}} \cdot \frac{1}{L_{WSS} \cdot L_{Circ} \cdot L_{ODN}} \cdot |H_{WSS}(f)|^2 \cdot |H_{WSS}(f)|^2 \\ & \cdot |H_{WSS}(f)|^2 \cdot |H_{WSS}(f)|^2 \Bigg] + \Bigg[hf_c(G_{boost} - 1)F \cdot \frac{G_{pre}}{L_2^{ROADM}} \\ & \cdot \frac{G_{boost}}{L_{metro}} \cdot \frac{G_{pre}}{L_3^{ROADM}} \cdot \frac{1}{L_{WSS} \cdot L_{Circ} \cdot L_{ODN}} \cdot |H_{WSS}(f)|^2 \\ & \cdot |H_{WSS}(f)|^2 \cdot |H_{WSS}(f)|^2 \cdot |H_{WSS}(f)|^2 \Bigg] \ldots \end{aligned} \quad (7)$$

where h is the Planck's constant, f_c is the carrier optical frequency, $F = 5$ dB is the noise figure of the EDFAs and L_i^{ROADM} is the total loss of each ROADM, combination of L_{WSS} and LOM, the insertion loss of the WSSs on the signal path (can be either one of two) and the optical matrix loss, respectively.

The 3 "degrees" in the 3D ROADM are assumed to be interconnected through a colorless, directionless and contentionless optical connection matrix. In the 2D ROADM, we assume the add/drop optical paths are dedicated to the coherent PON lambdas and are not connected to the optical matrix, but directly to the WSS_{drop} in DS or the WSS_{add} in US. In DS, the WSS_{drop} demultiplexes the coherent wavelength bundle and routes each lambda (through the SOA in the 2D version) towards the destination PON tree.

Fig. 11a shows the analytical scalability results for the DS direction at three different target BER_T, and for two bit rates. Assuming we want to achieve at least 29 dB L_{ODN}, as defined by the ITU-T standards [1] for class N1 PON, the results in this graphs show that at 400G in DS we can meet the requirement provided that the optical matrix loss is lower than 16 dB and that an advanced FEC with $BER_T = 10^{-2}$ or higher is used. The 200G speed based on PM-QPSK modulation is obviously more robust, and it can provide ODN loss above 30 dB for all the considered L_{OM} values even at the lowest $BER_T = 10^{-3}$. More in general, Fig. 11 (and the following one) are the main results of our paper, since they allow to perform scalability studies, trading off the different parameters. For instance, to achieve very high L_{ODN}, e.g. larger than 35 dB, the lower range of L_{OM} values should be considered at 400G, whereas both L_{ODN} and L_{OM} can be set within the higher values range considered in our study when the target bit rate is 200G. The inflection point of the curves in Fig. 11a at about 14 dB L_{OM} is due to the fact that the EDFA on the drop path of the ROADM is not able to compensate

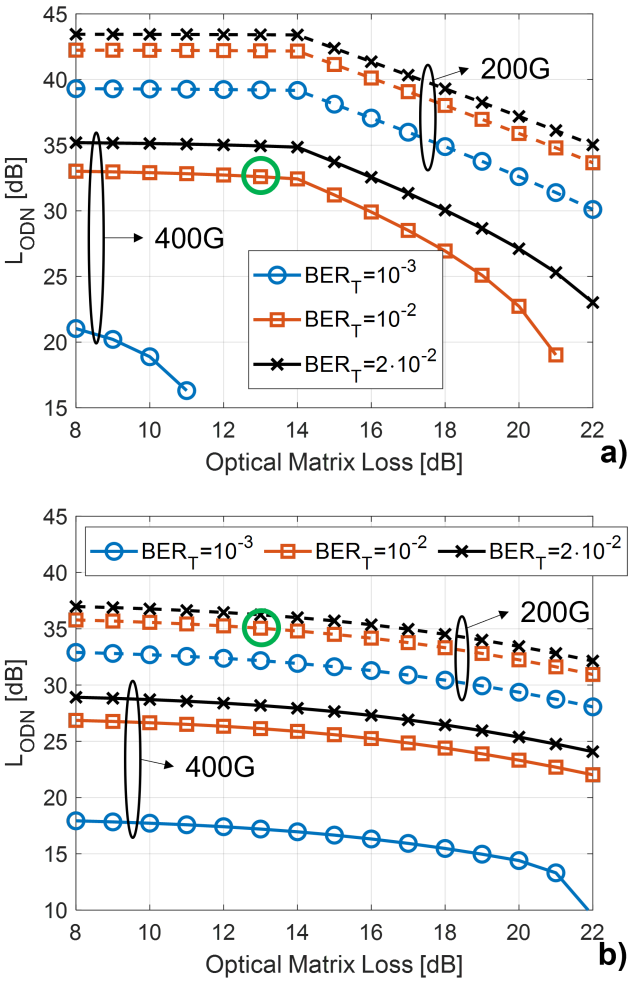

Fig. 11. ODN loss as a function of the optical matrix loss for 400G PM-16QAM (solid) and 200G PM-QPSK (dashed) and for $BER_T = 10^{-3}$ (blue, circles), $BER_T = 10^{-2}$ (red, squares) and $BER_T = 2 \cdot 10^{-2}$ (black, crosses). a) "3D D-ARCH" DS and b) "3D D-ARCH" US. The green circles indicate the operating conditions analyzed in Section 5.

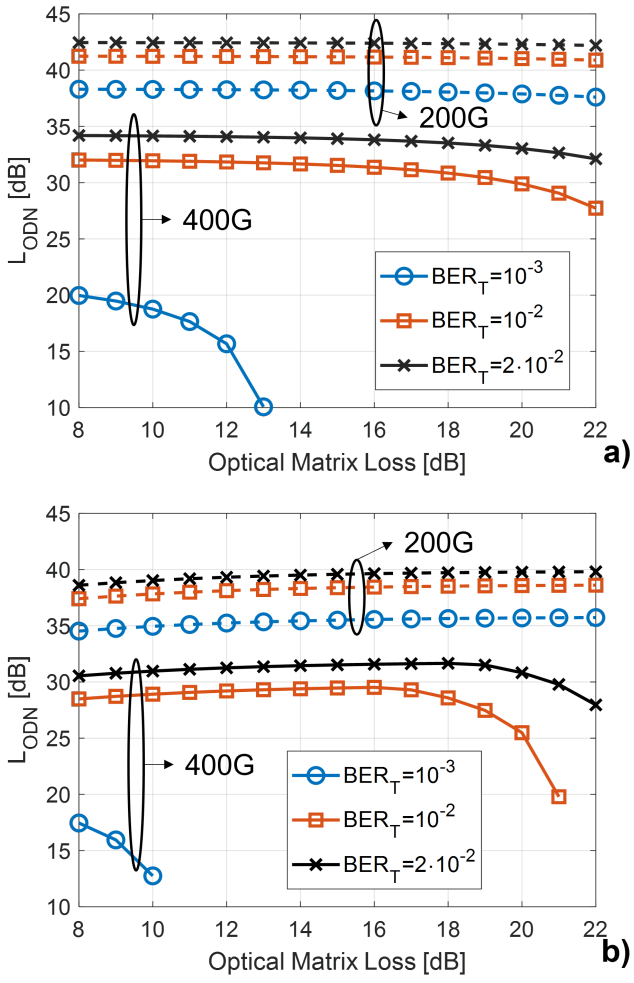

Fig. 12. ODN loss as a function of the optical matrix loss for 400G PM-16QAM (solid) and 200G PM-QPSK (dashed) and for $BER_T = 10^{-3}$ (blue, circles), $BER_T = 10^{-2}$ (red, squares) and $BER_T = 2 \cdot 10^{-2}$ (black, crosses). a) "2D D-ARCH" DS and b) "2D D-ARCH" US.

for the overall loss of the signal, thus each additional dB of attenuation introduced by the optical matrix results in an equal reduction of the total L_{ODN}. In our analysis, the gain of this EDFA is set to a maximum of 30 dB (as indicated for the preamp EDFA in the datasheet of a commercial ROADM we used in [4]). Please note that for low values of the L_{OM} parameter, this gain can be lower, considering that the target launch power in the PON segment, after the circulator, is 11 dBm.

Regarding the US transmission in the "3D D-ARCH" scheme, Fig. 11b shows that the minimum 29 dB ODN loss cannot be ensured with the 400G target bit rate based on PM-16QAM modulation, regardless of the considered BER threshold. At 200G, on the other hand, a FEC with 10^{-2} threshold or higher can enable ODN loss above the 29 dB limit for any considered L_{OM} value. Also a lower 10^{-3} FEC threshold can be used, provided that the matrix loss is lower than 19 dB. In this US case, the preamp EDFA on the add path of the ROADM has a maximum gain of 27 dB as per the commercial device datasheet. Moreover, we limit its maximum output power to 11 dBm, assuming 10 λs coming from the PON, each with 1 dBm average optical power, thus imposing a balanced optical power per channel and have at the output of the ROADM $P_{metro} = 0$ dBm for each channel, whether it is coming from the PON or the metro network. Here, we point out that a comprehensive analysis of the wavelength allocation is out of the scope of this work, but can be of great interest and will be the focus of further developments of the present analysis.

We believe that the results shown in the Figures of this Subsection are very interesting, showing for instance that in a metro+PON network based on deployed PON ODN with very high loss (29+ dB) a 400G DS and 200G US transmission per wavelength can be envisioned, a performance that greatly surpasses the current capability of legacy IM-DD systems, and can be achieved only thanks to the potentialities of DSP-based coherent transceivers.

In Fig. 11a and Fig. 11b the green circle at $BER_T = 10^{-2}$ and $L_{OM} = 13$ dB indicates the operating point of the "3D D-ARCH" scheme in DS and US that we further analyze in Sect. 5 through a statistical Montecarlo approach to evaluate the effect of non

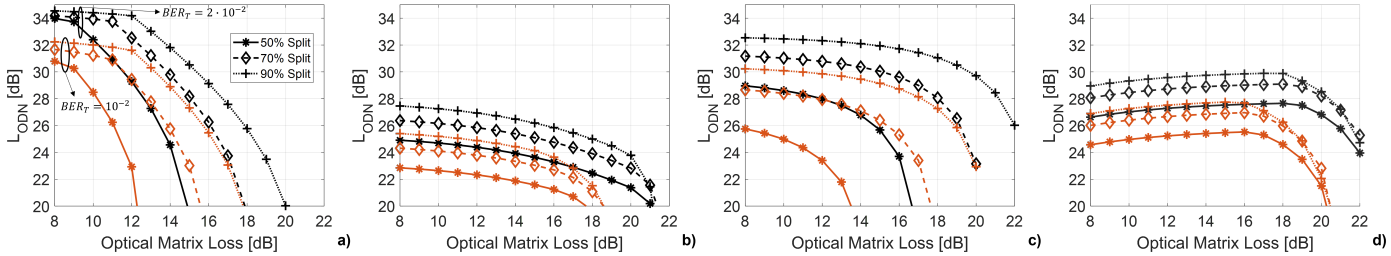

Fig. 13. ODN loss as a function of the optical matrix loss for 400G PM-16QAMK at $BER_T = 10^{-2}$ (red) and $BER_T = 2 \cdot 10^{-2}$ (black) for 50% split ratio (solid, circles), 70% split ratio (dashed, diamonds), 90% split ratio (dotted, plus signs). a) "3D E-ARCH" DS, b) "3D E-ARCH" US, c) "2D E-ARCH" DS and d) "2D E-ARCH" US.

perfect alignment between the central frequency of the signal and that of the WSSs in different optically bandlimited scenarios.

Fig. 12 shows the analytical results for the "2D D-ARCH" architecture, both in the DS and US direction. In this case, the SOA gain G_{SOA} is set to a maximum of 15 dB, but has a better impact than the preamp EDFA in the "3D" configuration because it has to amplify only a single λ rather than the whole bundle. Moreover, the signal goes through only one optical connection matrix (the one included in the central ROADM). Thus, in the DS transmission the inflection point cannot be observed anymore and the L_{ODN} vs. L_{OM} curves are much flatter. As a result, at 400G, the maximum acceptable matrix loss to achieve more than 29 dB ODN loss is increased to 20 dB at $BER_T = 10^{-2}$. However, again the lowest considered FEC threshold cannot ensure satisfactory performance. Conversely, for the 200G solution very high ODN loss over 38 dB can be obtained with any FEC, and up to 43 dB L_{ODN} are enabled by the SD-FEC for any given L_{OM}.

Very good results can be obtained again for the 200G solution in US transmission, as highlighted in Fig. 12b. Here, a somewhat counter-intuitive behavior can be observed, with the ODN loss increasing slightly with the optical matrix loss. This can be explained by the fact that the gain of the first booster EDFA encountered by the US signal is driven by the metro signal power at its input. When L_{OM} is low, this signal has a fairly high power, as it is attenuated only by the two WSS, inside the ROADM. When this happens the gain of the booster EDFA G_{boost} is low and thus the US signal coming from the PON is less amplified. In this case a slight power imbalance at the output of the ROADM can take place, between the power of the PON λs and the power of the metro channels, that might require a careful equalization of the channels power to enhance the system desing. As the connection matrix loss increases, also G_{boost} and, as a consequence, the PON channels undergo a higher gain and the received power increases. This can also be observed on the curves for 400G transmission, up to the point where the ASE introduced by the booster EDFA is so high that the sensitivity curves for the PM-16QAM case start to be affected and the L_{ODN} decreases. Theoretically, 400G transmission with $L_{ODN} > 29$ dB is still possible, at least for $BER_T = 2 \cdot 10^{-2}$, but the margin is very small and might not be enough to account for the filtering effects that we will investigate in Section 5.

In conclusion, from an overall system point of view, the "2D D-ARCH" architecture may be of interest when, besides the target of 400G DS and 200G US transmission per wavelength, also an ODN loss belonging to the highest ITU-T classes (31, 33 or 35 dB ODN loss) and high L_{OM} must be reached.

C. Scalability Analysis for the Evolutionary Architectures

In this Subection, we apply the analytical model to the evolutionary architecture presented in Section 3, again in both the "3D" and "2D" variants, to illustrate the performance scalability of a metro+PON solution coexisting with legacy PON technologies. The approach is the same followed in the previous Section 4B. The main physical layer difference with the "disruptive" scheme is the presence of an optical splitter/coupler in the enhanced access node, used to enable the correct routing of the ultra-high speed coherent US/DS wavelengths not only to the PON trees (as in the disruptive architecture) but *also* to a coherent transceiver that feeds the traffic to a legacy electronic access switch (using TDM/TDMA multiplexing). In this proposed architecture, some ONUs will work only on legacy PON standards, while some others are equipped with "premium" ONU coherent transceivers. We observe here, for instance on the DS path, that the splitter output going towards the PON tree will be much more critical in terms optical loss budget compared to the one going towards the electronic switch coherent receiver as the OLTs here would regenerate the signal through optical-to-electrical-to-optical conversion and amplification before sending it to the legacy ONUs. Thus, a properly designed asymmetrical splitting factor may largely improve the performance, by introducing less attenuation on the PON path, as we discuss in the following.

Fig. 13 shows L_{ODN} as a function of L_{OM} for the 400G PM-16QAM case and for different BER_T (and different split ratios in the asymmetrical 1x2 aforementioned splitter/combiner) in the 4 considered transmission schemes: "3D" DS, "3D" US, "2D" DS and "2D" US. The split ratio is defined as percentage of power that is used, at the splitter/coupler, for the coherent PON wavelength. For instance a 90% split ratio means that at the splitter/coupler an extra loss is considered for the coherent signal equal to $L_{split,dB} = |10 \cdot log_{10}(90/100)| + 1$, where the +1 dB factor is added to take into account a (quite conservative) value for the excess loss of the splitter/coupler. The "3D" scheme in DS provides the highest possible L_{ODN}, since about 32 dB and 34 dB can be achieved for $BER_T = 10^{-2}$ and $BER_T = 2 \cdot 10^{-2}$ respectively, but only for a limited range of L_{OM} values up to 12 dB and 13 dB, respectively for 70% and 90% split ratio (Fig. 13a). The same "3D solution" is again unable to provide sufficient ODN loss to comply with the current PON standards at 400G speed in US (Fig. 13b). Fig. 13c and Fig. 13d confirm that the "2D" solution is slightly more robust to the optical matrix loss, but it cannot provide acceptable L_{ODN} margins above the 29 dB, especially in the US case. Much better performance can be achieved in the 200G summarized in Fig. 14. In the "3D" DS case (Fig. 14a) even a very low 50% split ratio can in principle be

tolerated with L_{ODN} values in excess of 29 dB for L_{OM} up to 16 dB when $BER_T = 10^{-3}$. The US case is, as usual, more critical, and requires the use of a higher FEC threshold. Nevertheless, for $BER_T = 10^{-2}$ even a 50% split can be included. Regarding the "2D" option very good ODN loss greater than 29 dB can be achieved in nearly all the analyzed cases. Only the DS with 50% split and $BER_T = 10^{-3}$ yields a lower L_{ODN} for $L_{OM} > 20$ dB, a rather unrealistic value. Both Fig. 13d and Fig. 14d for the "2D E-ARCH" case in US show an increasing L_{ODN} with the optical matrix loss for the same reasons discussed in the "2D D-ARCH" US case shown in Fig. 12b. In all respects, Fig. 13 and Fig. 14 show that any additional attenuation at the splitter/coupler location reduces the maximum achievable ODN loss by an equal amount.

5. DISCUSSION ON OTHER POSSIBLE IMPAIRMENTS

In this Section, we discuss a potential source of additional impairment in a metro+PON scenario related to the filtering effects associated with the WSSs inside the ROADMs.

We have analyzed in detail experimentally, analytically and through simulations the filtering effect of ROADMs on the performance of "Vendor 3" TRX also in our previous paper on filtering penalties [18]. Here, we extend the analysis to the other two TRXs and apply the analytical model to the statistical study of some of the previously proposed metro+PON configurations. Fig. 15 shows the sensitivity penalty as a function of the OSNR for several values of the ratio between the bandwidth B of the supergaussian (SG) filter (that for the experimental part was implemented through the WaveShaper filter shown in Fig. 8) and the symbol rate R_S. We assume a SG filter of order 3, since we experimentally verified it better resembles the actual spectral shape of WSSs. As expected, the penalty increases for decreasing OSNR and for decreasing filter bandwidth and does so, with a nearly identical trend for the three TRX. For instance, for about 20 dB OSNR and $B/R_S = 0.9$ (which, for instance, at 64 Gbaud corresponds to a filter 3dB bandwidth equal to about 57 GHz) the penalty is about 2 dB for the three devices. This penalty, obtained for a perfect alignment between the central frequency of the filter and that of the transmitted signal, would translate in a net reduction of the achievable L_{ODN} shown in the previous Section, for the various considered cases. Moreover, Fig. 15 shows a very good match of the analytical model with the experimental results (circles). Consequently, in Fig. 16 we show the results of an analytical statistical study of the estimated sensitivity penalty for the "3D D-ARCH" scheme, for 400G DS and 200G US communication (in the conditions indicated by the green circles in Fig. 11a and Fig. 11b). For consistency with the previous Sections, the study is again conducted considering the "Vendor 3" TRX. For each WSS bandwidth, we generated in a Monte-Carlo simulation, 1000 realizations of the filter supergaussian profile varying the central frequency within ±5% of the nominal bandwidth of the filter ($\Delta f_c \in [-5\%, +5\%] \cdot B$) following a uniform distribution. Fig. 16 shows the probability distribution for the ODN loss penalty with respect to the maximum computed ODN loss for several B/R_S ratios when the filter order is 3 and $BER_T = 10^{-2}$. For the 400G DS configuration (Fig. 16a), we show only the comparison between $B/R_S = 150\%$ and $B/R_S = 125\%$ as a lower WSS bandwidth results in a BER always greater then $BER_T = 10^{-2}$. When $B/R_S = 125\%$ the ODN loss penalty distribution shows a peak at about 2.2 dB. In the 200G transmission case (Fig. 16b), we do not show results for $B/R_S = 125\%$ as they are nearly identical to the $B/R_S = 150\%$ case. As we presented in the previous Sections, the PM-QPSK modulation for 200G is much more resilient to impairments as confirmed by the statistical results for $B/R_S = 100\%$, showing a peak of the ODN loss penalty distribution at about 1.7 dB. The penalty shown in the x-axis in Fig. 16 is a net reduction in dB of the performance shown in the previous Section, when no optical filtering effect was taken into account.

6. DISCUSSION AND CONCLUSIONS

We have presented a general framework and several examples of the scalability of metro+PON, all-optical and edge ROADM-routed networks. As previously stated, this work is to be meant as a vast but preliminary study in this field and is focused on establishing the "rules of thumb" in terms of scalability, given commercial coherent transceiver current performance and the typical losses and noise inside ROADMs. Our present work should be the starting point for further studies, such as:

- techno-economics: when and if coherent transceivers and ROADMs cost will be compatible with the access scenario (even considering super-users as discussed in Section 1).
- how to implement efficiently multiple access in the upstream using burst-mode TDMA coherent TRX. Burst mode operation in EDFA is today not typical but it was largely studied in the past at the research level in many projects dealing with all-optical packet switched networks [17].
- as an alternative, the option of implementing Digital Sub-Carrier Multiplexing, as proposed in [6] and [7] also in this scenario can be very interesting, since it would allow to use the *same* wavelength in both US and DS and for both segments (PON on a single fiber bidirectionally, and

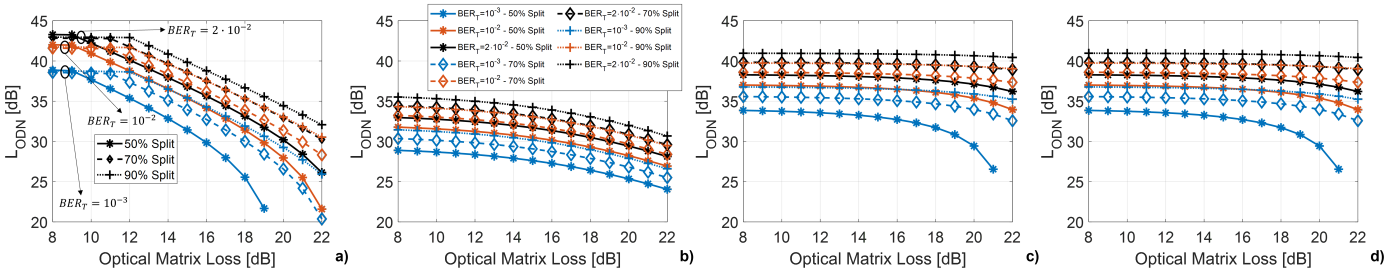

Fig. 14. ODN loss as a function of the optical matrix loss for 200G PM-QPSK at $BER_T = 10^{-3}$ (blue), $BER_T = 10^{-2}$ (red) and $BER_T = 2 \cdot 10^{-2}$ (black) for 50% split ratio (solid, circles), 70% split ratio (dashed, diamonds), 90% split ratio (dotted, plus signs). a) "3D E-ARCH" DS, b) "3D E-ARCH" US, c) "2D E-ARCH" DS and d) "2D E-ARCH" US.

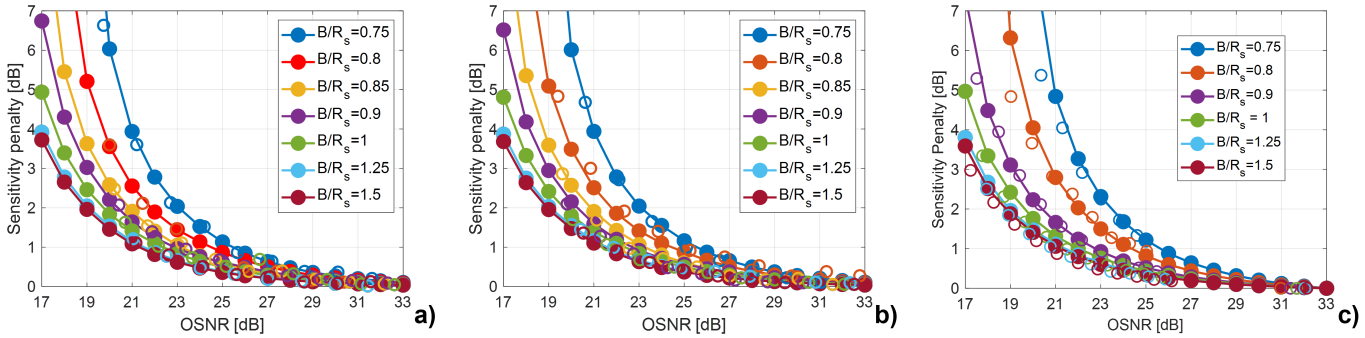

Fig. 15. Experimental (circles) and analytical (solid, dots) sensitivity penalty vs OSNR for several B/R_S ratios and a) "Vendor 1", b) "Vendor 2" and c) "Vendor 3" TRX, for 63 GBaud PM-16QAM transmission. "Vendor 3" TRX results in c) are taken from [18].

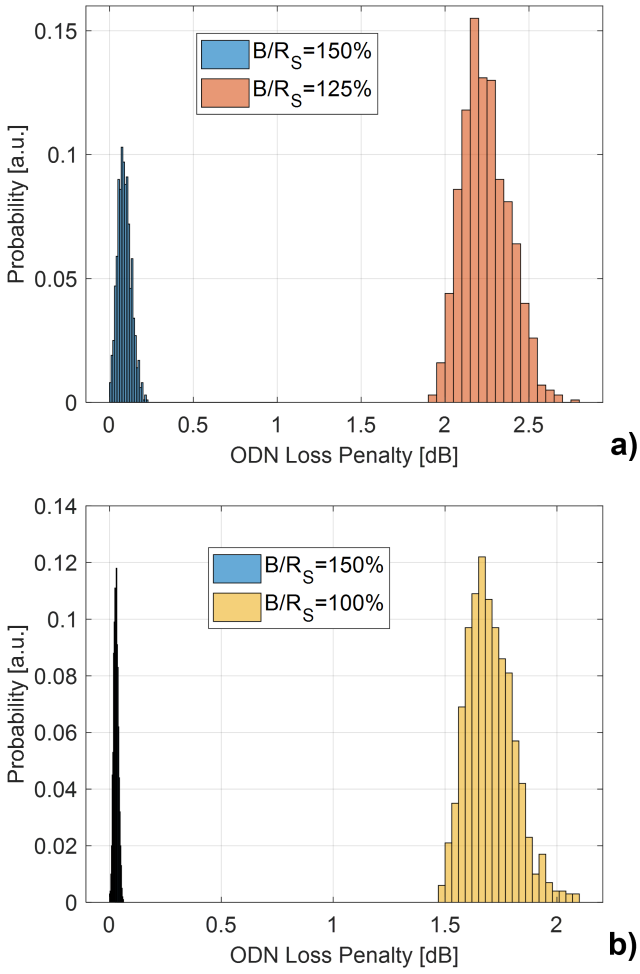

Fig. 16. Histograms of the ODN loss penalty due to non centered optical filtering for a) 400G "3D diruptive" DS and b) 200G "3D diruptive" US scheme when $L_{OM} = 13$ dB, $BER_T = 10^{-2}$, $\Delta f_c \in [-5\%, +5\%] \cdot B$ and for $B/R_S = 150\%$ (blue), $B/R_S = 125\%$ (red), $B/R_S = 100\%$ (yellow).

metro on two fibers in the typical horseshoe configuration [19]). Moreover, the network would benefit from increased flexibility enabling dedicated power management for each subcarrier.

- the analysis of several second order physical layer effects that were not treated in this paper, such as fiber Kerr effects (which anyway should be limited due to the relatively short fiber distances to be covered), optical amplifier gain and noise figure tilt, optical crosstalk in the ROADMs and optical backreflections in the bidiretional PON.

- lastly, the proposed metro+PON architecture would also need a complete re-design of the higher network layers.

ACKNOWLEDGMENTS

This work was carried out in the TIM laboratory and in the PhotoNext Center facilities at Politecnico di Torino (www.photonext.polito.it) under a research collaboration with Telecom Italia (TIM). This work was also supported by the EU Horizon Europe framework under project ALLEGRO No. 101092766 . Mrs. Casasco's PhD is sponsored by TIM.

REFERENCES

1. "50-Gigabit-capable passive optical networks (50G-PON): Physical media dependent (PMD) layer specification," ITU-T G.9804.3.
2. P. Torres-Ferrera, F. Effenberger, M. S. Faruk, S. J. Savory and R. Gaudino, "Overview of high-speed TDM-PON beyond 50 Gbps per wavelength using digital signal processing," *IEEE Journal of Optical Communications and Networking*, vol. 14, no. 12, pp. 982-996, December 2022, 2022.
3. Y. Luo and F. Effenberger, "What is beyond 50G: future standards of optical access networks [Invited]," *IEEE Journal of Optical Communications and Networking*, vol. 16, no. 7, pp. C106-C112, 2024.
4. G. Rizzelli, et al., "Experimental Demonstration of In-Field 400G Coherent Metro-Access Convergence," in *Proc. of Optical Fiber Communications Conference (OFC)*, San Diego CA, 2024.
5. G. Rizzelli and R. Gaudino, "Planning tools for next-generation DSP-based passive optical networks above 50G [Invited Tutorial]," *IEEE/OPTICA Journal of Optical Communications and Networking*, vol. 16, no. 7, pp. C88-C96, 2024.
6. H. Wang et al., "Fast-Convergence Digital Signal Processing for Coherent PON Using Digital SCM," *IEEE/OPTICA Journal of Lightwave Technology*, vol. 41, no. 14, pp. 4635-4643, 15 July15, 2023.
7. G. Simon et al., "200 Gb/s Coherent Point-to-Multipoint Coexistence With 50G-PON for Next-Generation Optical Access," *IEEE Photonics Technology Letters*, vol. 36, no. 10, pp. 665-668, 15 May15, 2015.

8. G. Rizzelli *et al*., “Scaling Laws for Unamplified Coherent Transmission in Next-Generation Short-Reach and Access Networks,” *IEEE J. of Light. Techn.*, vol. 39, no. 18, pp.5805-5814, 2021.
9. G. Rizzelli and R. Gaudino, “Sensitivity and Scaling Laws of Unamplified Coherent Architectures for Intra-Data Center Links Beyond 100 Gb/s,” in *2019 21st Intern. Conf. on Transparent Optical Networks (ICTON)*, Angers, France, 2019.
10. B. Zhang, C. Malouin, and T. Schmidt, “Design of coherent receiver optical front end for unamplified applications,” *Opt. Exp.*, vol. 20, pp. 3225–3234, 2012.
11. G. Rizzelli, P. Torres-Ferrera and R. Gaudino, “An Analytical Model for Coherent Transmission Performance Estimation After Generic Jones Matrices,” *Journal of Lightwave Technology*, vol. 41, no. 14, pp. 4582-4589, 2023.
12. G. Rizzelli, P. Torres-Ferrera, F. Forghieri and R. Gaudino, “An Analytical Model for Performance Estimation in Modern High-Capacity IMDD Systems,” *Journal of Lightwave Technology*, vol. 42, no. 5, pp. 1443-1452, 2024.
13. G. Rizzelli and R. Gaudino, “Analytical Performance Estimation Methods for Modern Optical Communications systems,” in *Proc. of Photonics Global Conference (PGC)*, Stockholm, Sweden, 2023, pp. 27-31.
14. P. Torres-Ferrera, G. Rizzelli, A. Napoli and R. Gaudino, “Filtering Power Penalty Evaluation of Coherent Systems Affected by ASE and Transceiver Noise,” in *Proc. of Optical Network Design and Modelling (ONDM)*, Madrid, Spain, 2024, pp. 1-3.
15. Robert F.H. Fischer, “Linear Equalization,” *Precoding and Signal Shaping for Digital Transmission*, New York, NY, USA: Wiley-Interscience, 2002, ch. 2, sec. 2.2.4, pp. 35-43.
16. “Spectral grids for WDM applications: DWDM frequency grid,” ITU-T G.694.1.
17. A. Bianciotto, A. Carena, V. Ferrero and R. Gaudino, “EDFA gain transients: experimental demonstration of a low cost electronic control,” *IEEE Photonics Technology Letters*, vol. 15, no. 10, pp. 1351-1353, Oct. 2003.
18. G. Rizzelli, P. Torres-Ferrera, A. Napoli and R. Gaudino, “Filtering Effects Characterization in Metro-Access Networks and Future High-Speed Coherent Optical Communication Schemes,” *Journal of Lightwave Technology*, submitted, June 2024, 2024.
19. M. M. Hosseini, J. Pedro, A. Napoli, N. Costa, J. E. Prilepsky and S. K. Turitsyn, “Optimized design of filterless horseshoe networks exploiting point-to-multipoint coherent transceivers,” in Journal of Optical Communications and Networking, vol. 15, no. 9, pp. 569-578, September 2023, 2023.